



Cite this: DOI: 10.1039/c6cp07200c

# Synthesis and EPR-spectroscopic characterization of the perchlorotriarylmethyl tricarboxylic acid radical (PTMTC) and its $^{13}\text{C}$ labelled analogue ( $^{13}\text{C}$ -PTMTC)†

Marwa Elewa,‡<sup>ab</sup> Nadica Maltar-Strmečki,‡§<sup>c</sup> Mohamed M. Said,<sup>b</sup>  
Hosam A. El Shihawy,<sup>b</sup> Mohamed El-Sadek,<sup>d</sup> Juliane Frank,<sup>a</sup> Simon Drescher,<sup>a</sup>  
Malte Drescher,<sup>e</sup> Karsten Mäder,<sup>a</sup> Dariush Hinderberger\*<sup>c</sup> and Peter Imming\*<sup>a</sup>

A hydrophilic tris(tetrachlorotriaryl)methyl (tetrachloro-TAM) radical labelled 50% with  $^{13}\text{C}$  at the central carbon atom was prepared. The mixture of isotopologue radicals was characterised by continuous wave and pulsed X-band electron paramagnetic spectroscopy (EPS). For the pharmaceutical and medical applications planned, the quantitative influence of oxygen, viscosity, temperature and pH on EPR line widths was studied in aqueous buffer, DMSO, water–methanol and water–glycerol mixtures. Under *in vivo* conditions, pH can be disregarded. There is a clear oxygen dependence of the width of the  $^{12}\text{C}$  isotopologue single EPR line in aqueous solutions while changes in rotational motion (viscosity) are observable only in the doublet lines of the central carbon of the  $^{13}\text{C}$  isotopologue. The tetrachloro-TAM proved to be very stable as a solid. Its thermal decay was determined quantitatively by thermal annealing. Towards ascorbic acid as a reducing agent and towards an oocyte cell extract it had a half-life of approx. 60 and 10 min. Thus for *in vivo* applications, 50%  $^{13}\text{C}$  tetrachloro-TAMs are suitable for selective and simultaneous oxygen and macroviscosity measurements in a formulation, e.g. nanocapsules.

Received 20th October 2016,  
Accepted 8th February 2017

DOI: 10.1039/c6cp07200c

rsc.li/pccp

## 1 Introduction

Electron paramagnetic resonance (EPR/ESR, electron spin resonance) spectroscopy is a magnetic resonance method to detect and characterize paramagnetic species with unpaired electrons. In the context of (bio)medical applications, EPR has shown its

usefulness for the exploration of the microenvironment of a spin probe with respect to molecular oxygen concentrations, micro-polarity, microviscosity, and pH.<sup>1–3</sup> EPR-based imaging (EPRI) has been used to observe the distribution of free radicals in biological systems.<sup>4,5</sup> However, *in vivo* EPRI is hampered by the lack of metabolically stable, non-toxic spin probes. Moreover, for meaningful *in vivo* measurements the signal needs to be strong and resolved to a degree that allows distinguishing which of the various microenvironmental parameters cause the observed effects in the EPR signal.

The Gomberg radical, *viz.* the unsubstituted triarylmethyl (TAM) radical,<sup>6</sup> dimerizes in solution<sup>7,8</sup> and is quickly oxidized.<sup>9–11</sup> The multiple splitting of the EPR signal results from electron spin-hydrogen nuclear spin hyperfine couplings and reduces signal intensity pronouncedly. So for *in vivo* EPR applications, a stable radical with a single strong line, e.g., a member of the tris(tetrathiaphenyl)methyl radicals, would be ideal in terms of intensity. At the same time, the information content of a single line, *i.e.* an isotropic spectrum, is low. A change in line width, for instance, cannot be ascribed to a particular microenvironmental parameter easily, but may result from changes of several parameters (e.g. viscosity and oxygen concentration). Tetrathiatriarylmethyl radicals were synthesized and thoroughly investigated in terms of their applicability for oxygen measurements and other purposes enlisted above.

<sup>a</sup> Institut für Pharmazie, Martin-Luther-Universität Halle-Wittenberg, Wolfgang-Langenbeck-Str. 4, 06120 Halle, Germany.

E-mail: peter.imming@pharmazie.uni-halle.de

<sup>b</sup> Faculty of Pharmacy, Suez Canal University, P.O. 41522, Ismailia, Egypt

<sup>c</sup> Institut für Chemie, Physikalische Chemie, Martin-Luther-Universität Halle-Wittenberg, Von-Danckelmann-Platz 4, 06120 Halle, Germany.

E-mail: dariush.hinderberger@chemie.uni-halle.de

<sup>d</sup> Faculty of Pharmacy, Zagazig University, Zagazig, Egypt

<sup>e</sup> Department of Chemistry and Konstanz Research School Chemical Biology, University of Konstanz, 78457 Konstanz, Germany

† Electronic supplementary information (ESI) available: Syntheses; ratio of peak-to-peak intensities of central  $^{12}\text{C}$  line and  $^{13}\text{C}$  doublet lines; dependence of 1/TM relaxation rate on water/methanol compositions, influence of temperature on  $^{13}\text{C}$ -PTMTC line width; ascorbic acid reduction assay. See DOI: 10.1039/c6cp07200c

‡ Author contributions: M. E. and N. M. S. contributed equally. M. E. did the syntheses. N. M. S., M. E., J. F. and S. D. performed the EPR and related experiments. M. D. performed the oocyte experiment. M. E. and N. M. S. wrote a first draft. P. I. and D. H. wrote the manuscript with input from K. M., M. M. S., H. A. El-E. and M. El-S. edited the manuscript.

§ Present address: Ruđer Bošković Institute, Division of Physical Chemistry, Bijenička c. 54, 10000 Zagreb, Croatia.

Tris(tetrachlorotriaryl)methyl (tetrachloro-TAM) radicals, in which the hydrogen atoms on the aromatic ring were replaced with bulky chlorine atoms, were reported as early as 1967.<sup>12</sup> Steric shielding of the central methyl carbon by the six *ortho*-chlorine atoms is responsible for high chemical and thermal stability of these radicals.<sup>13–15</sup> Some applications were reported for radicals of the tetrachloro-TAM family such as imaging of oxygen concentration in tissue,<sup>16,17</sup> detection of superoxide radical anion,<sup>18–20</sup> detection of hydroxyl radical,<sup>21</sup> spin labelling of amino acids and peptides,<sup>22</sup> and their usefulness for dynamic nuclear polarization (DNP)<sup>23–25</sup> and material science.<sup>26–29</sup>

The EPR spectra of the tetrachloro-TAM radicals, *e.g.*, the perchlorotriarylmethyl tricarboxylic acid (**PTMTC**) radical, show the intensive single peak typical of TAM radicals substituted in such a way as to minimize electron–nuclear coupling. The peak is accompanied by three symmetrical pairs of satellite peaks stemming from hyperfine coupling with natural abundance <sup>13</sup>C at the *ipso*, *ortho*, *para* and *meta* positions of the phenyl rings, Fig. 1A. Surprisingly, hyperfine coupling to the central carbon displayed low intensity under the conditions of the EPR measurement (no influence on the central line; below saturation limit). Paniagua *et al.*<sup>30</sup> attributed this fact to fast relaxation because of the slow tumbling rate of the radical in the solvent used (H<sub>2</sub>O/DMSO = 1/1, V/V).

We wanted to explore further when and how hyperfine coupling of the unpaired electron (formally located at the central carbon) occurs with the central carbon atom nuclear spin. To this end, we needed to prepare a tetrachloro-TAM radical labelled with <sup>13</sup>C at the position in question. At the same time, we planned to exploit the increased spectral information that is inherent in the coupling pattern and its interaction with the microenvironment. For this, we chose to enrich the methyl radical center by 50% <sup>13</sup>C only. Through this, we would simultaneously observe two radical species, **PTMTC** and <sup>13</sup>C-**PTMTC**, that behave identically regarding chemical stability, solubility, chromatographic properties, and biodistribution. One would expect to detect the spectral

superposition of the single strong EPR line of the <sup>12</sup>C species, accompanied by the high field and low field peaks of the <sup>13</sup>C labelled species, Fig. 1B. Here, we report the synthesis of this mixture of isotopologue TAM radicals and characterize the impact of some parameters mimicking physiological conditions, *e.g.*, variation of viscosity, pH, and oxygen content.

While <sup>14</sup>N, <sup>15</sup>N isotope-enriched or -depleted nitroxide radicals were studied intensively, reports on <sup>13</sup>C-enriched trityl radicals are limited to estimates of electron and spin density distributions, information about the anisotropic hyperfine interactions, and ENDOR studies, using triphenyl[<sup>13</sup>C]methyl and deuterated analogues. We here present not only the spectroscopic and physical-chemical characterization but also explore the capability to employ the **PTMTC** radical and its isotopologue in functional *in vitro* model systems and from *in vivo* studies under more complex conditions. These radicals are known to be toxic. However, they are also reduced quickly in cell lysates (see below). If they are released slower from the lipophilic formulations we published than they are reduced after release, toxicity will probably not become an issue.

## 2 Experimental methods

### 2.1. Materials and general methods for synthesis and analytical characterization

Commercial chemicals used for the synthesis were used without further purification unless stated otherwise. Buffer salts were obtained from Gruessing (Filsum, Germany). Glycerol was obtained from VWR International (Fontenay-sous-Bois, France). <sup>13</sup>C labelled chloroform was purchased from Cambridge Isotope Laboratories Inc. Water was used in doubly distilled quality.

### 2.2. General methods for synthesis and analytical characterization

All organic solvents were distilled and dried before use and stored over molecular sieves (3 Å). Glassware for reactions

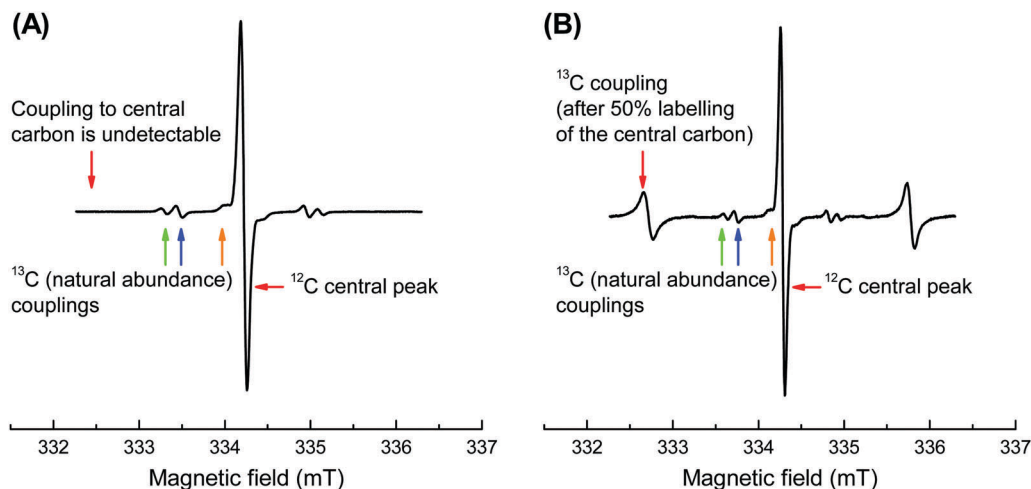


Fig. 1 EPR spectra of **PTMTC** and <sup>13</sup>C-**PTMTC** radical in phosphate buffer, pH 7.4 (*c* = 1 mM). (A) **PTMTC** appears as a single line (<sup>12</sup>C central peak), accompanied by natural abundance <sup>13</sup>C satellite couplings. (B) The <sup>12</sup>C central peak of **PTMTC** and the doublet of <sup>13</sup>C-**PTMTC** stemming from the hyperfine coupling to the <sup>13</sup>C nuclei (*I* = 1/2), again accompanied by <sup>13</sup>C natural abundance couplings.

under argon atmosphere was oven-dried at 100 °C for 2 h prior to use, evacuated, and flushed with argon immediately. The purity of all compounds and the progress of reactions were monitored by thin layer chromatography (TLC) using silica gel 60 F<sub>254</sub> plates (Merck KGaA, Darmstadt, Germany). Visualizations were accomplished with a UV lamp (254 nm) or iodine staining, and the *R<sub>f</sub>* values given are uncorrected. Purification of the compounds was achieved either by crystallization from appropriate solvents or flash chromatography. Melting points (Mp) were determined with a Boethius apparatus. NMR spectra were recorded on an Agilent Technologies VNMRS 400 MHz (Agilent Technologies, Böblingen, Germany). Chemical shifts ( $\delta$ ) are reported in parts per million (ppm) relative to TMS. The splitting pattern was assigned as follows: s = singlet, bs = broad singlet, d = doublet, t = triplet, q = quartet, m = multiplet and coupling constants (*J*) are given in Hertz (Hz). <sup>13</sup>C NMR chemical shifts were reported as  $\delta$  values (ppm) relative to the residual nondeuterated solvent peak in the corresponding spectra (chloroform  $\delta$  = 77.2, methanol  $\delta$  = 49.0, DMSO  $\delta$  = 39.5). Mass spectrometry (MS): Electron spray ionization (ESI) mass spectra were recorded on a LCQ Classic (Thermo Finnigan, San Jose, California, USA). Electron impact (EI) mass spectra were recorded on an AMD 402 (AMD Intectra GmbH, Harpstedt, Germany) with a medium ionization voltage of 70 eV. High-resolution mass spectra were recorded on an orbitrap XL mass spectrometer (Thermo Fisher Scientific) with a resolving power of 100 000 at *m/z* 400, samples were introduced to the MS by static nano-electrospray ionization (ESI). Mass calculations were done for the isotope peak with the highest intensity. Infrared spectra (IR) spectra were recorded on an IFS 28 FTIR spectrometer (Bruker, Billerica, USA) with a Thermo Spectra-Tech ATR unit (Thermo Scientific).

### 2.3. Sample preparation for EPR spectroscopic characterization

The hydrophilic radicals perchlorotriarylmethyl tricarboxylic acid (PTMTC) radical and its <sup>13</sup>C analogue (<sup>13</sup>C-PTMTC) were dissolved (*c* = 1 mM) in phosphate buffer (PB 50 mM, pH 7.4). The effect of pH was studied with 1 mM solutions of <sup>13</sup>C-PTMTC in PB (50 mM, pH range from 0 to 14). The impact of viscosity was investigated with solutions of radicals PTMTC and <sup>13</sup>C-PTMTC (*c* = 1 mM) in a mixture of absolute glycerol and PB (50 mM, pH 7.4), the glycerol content ranging from 0% to 80% (m/m). Solutions of PTMTC and <sup>13</sup>C-PTMTC radicals (*c* = 1 mM) were prepared in a mixture of PB (50 mM, pH 7.4) and absolute methanol, the methanol content ranging from 0% to 100% (V/V). A solution of <sup>13</sup>C-PTMTC in glycerol/PB 50 mM, pH 7.4 (40/60, m/m) was selected to examine the relation between line width and the viscosity/temperature ratio. A solution of <sup>13</sup>C-PTMTC (*c* = 1 mM) in PB (50 mM, pH 7.4) was used to study both the thermal annealing within the temperature range 323–353 K and the stability against ascorbic acid. A solution of PTMTC in PB (50 mM, pH 7.4) was used to perform the cell-lysate study (*c* = 0.5 mM).

### 2.4. Measurements at defined oxygen contents

Measurements were conducted as described previously.<sup>31</sup> Briefly, PTMTC and <sup>13</sup>C-PTMTC buffer solutions were flushed with either pure nitrogen or defined mixtures of oxygen and nitrogen at a flow rate of 2 L min<sup>-1</sup> for 3 min using septum vials and cannulae. An anesthesia gas mixer with flow meter tubes (Dräger, Lübeck, Germany) provided defined gas mixtures. The partial pressure of oxygen (mmHg) in the gas above the solution was confirmed by a needle-type optical oxygen microsensor (Type PSt1, PreSens GmbH, Regensburg, Germany) directly after the EPR measurements. Oxygen content (%) in the gas above the solution was calculated assuming ambient pressure.

### 2.5. Continuous wave EPR (CW EPR) spectra

CW EPR spectra of <sup>13</sup>C-PTMTC were recorded on a Miniscope MS 400 benchtop spectrometer (Magnetech, Berlin, Germany) working at X-band frequencies ( $\nu_{mw}$  ~ 9.4 GHz). The microwave frequency ( $\nu_{mw}$ ) was recorded with a Racal-Dana frequency counter, model 2101 (Racal Instruments, Neu-Isenburg, Germany). The temperature was set and controlled within  $\pm 1$  K with a TC H03 (Magnetech, Berlin, Germany) control unit, using nitrogen gas flow. A manganese standard sample, Mn<sup>2+</sup> in ZnS (Magnetech, Berlin, Germany), was used to calibrate the magnetic field of the spectrometer. The spectra were simulated with a custom-built program in MATLAB (The MathWorks Inc., Natick, Massachusetts, USA) using the EasySpin program package for EPR.<sup>32</sup>

### 2.6. Pulse X-band EPR

Pulse X-band EPR studies were performed on an X-band Bruker ELEXSYS 580 spectrometer. The temperature was controlled by a closed cycle cryostat (ARS AF204). The phase memory time, *T<sub>M</sub>* were measured using a simple Hahn spin echo sequence:  $\pi/2$ - $\tau$ - $\pi$ - $\tau$ -echo. A microwave pulse length of 28 ns was used for a  $\pi/2$  pulse. An initial interpulse delay,  $\tau$ , of 400 ns and an increment of 8 ns were used. The standard four-step phase cycle procedure was applied to eliminate measurement artefacts from unwanted echoes. Relaxation curves have been fitted by monoexponential decay function.

## 3 Results and discussion

### 3.1. Synthesis of PTMTC and <sup>13</sup>C-PTMTC

The preparation of PTMTC has been reported before.<sup>33</sup> For this study, the preparation of PTMTC and the partially labelled <sup>13</sup>C-PTMTC (Fig. 2) was optimized regarding reaction time (45 min instead of 20 h), ease (no oleum, one-step instead of three-step procedure for triarylmethane formation), and yield (lit. 33 reported no yield; we reproducibly obtained the yields shown).

Perchlorotriarylmethanes (Fig. 2, **2a** and **2b**) were synthesized by Friedel–Crafts alkylation of 1,2,4,5-tetrachlorobenzene (**1**) with chloroform (CHCl<sub>3</sub>) in the presence of aluminum trichloride (AlCl<sub>3</sub>).<sup>34</sup> A mixture of CHCl<sub>3</sub> and <sup>13</sup>CHCl<sub>3</sub> (1:1 ratio) was used to prepare **2b**. Reaction of **2a** or **2b** with an excess of *n*-BuLi and tetramethylethylenediamine (TMEDA) in

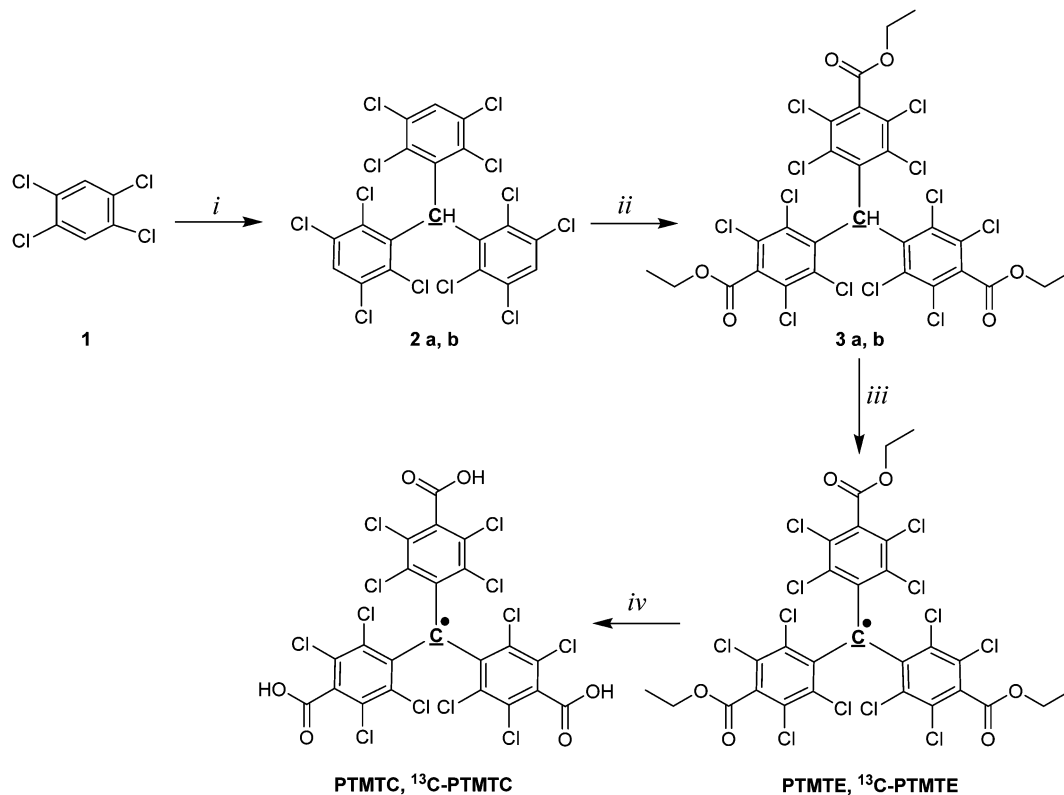


Fig. 2 Synthesis of **PTMTC** and  $^{13}\text{C}$ -**PTMTC** radicals. Reagents and conditions: (i)  $\text{CHCl}_3/^{13}\text{CHCl}_3$  (1 : 1 ratio)/ $\text{AlCl}_3/160^\circ\text{C}$ , 39%; (ii) *n*-BuLi, TMEDA, ethyl chloroformate, 79%; (iii) 1.  $\text{Bu}_4\text{NOH}$ , 2. *p*-Chloranil, 83%; (iv) 95%  $\text{H}_2\text{SO}_4$ , 85%; central carbon **C** is the 50%  $^{13}\text{C}$  labelled atom of  $^{13}\text{C}$ -**PTMTC**.

THF at low temperature gave the corresponding trianion. With ethyl chloroformate, the perchlorotriarylmethane triethyl esters (**3a** and **3b**) were formed<sup>18,31</sup> and were then converted to the triester radicals (**PTMTE** and  $^{13}\text{C}$ -**PTMTE**) by a two-step process: Conversion into the triaryl-carbanion with a 1 mM solution of tetra-*n*-butylammonium hydroxide ( $\text{Bu}_4\text{NOH}$ ) in methanol, followed by oxidation with *p*-chloranil.<sup>35</sup> This is different from the synthesis of the tris(tetrathiaphenyl)methyl triethyl ester radical that was released through the conversion of the corresponding methane derivative into the carbocation followed by reduction with stannous chloride.<sup>31</sup>

Heating **PTMTE** or  $^{13}\text{C}$ -**PTMTE** in concentrated sulfuric acid yielded the tricarboxylic acid radicals **PTMTC** and  $^{13}\text{C}$ -**PTMTC**.

### 3.2. EPR spectra

The naturally most abundant isotope of carbon,  $^{12}\text{C}$  (~98.9%) has a nuclear spin of  $I = 0$  and, hence, does not interact with the unpaired electron spin. The EPR spectrum of **PTMTC** accordingly showed a single peak, in addition to three symmetrical pairs of satellites because of hyperfine coupling with naturally abundant  $^{13}\text{C}$  (1.07%) at three different positions/types of carbon, Fig. 1A. The spectrum of the isotopically enriched analogue,  $^{13}\text{C}$ -**PTMTC**, displayed three primary EPR lines that are a superposition of the single line of  $^{12}\text{C}$ -isotopologue **PTMTC** and the doublet derived from the  $^{13}\text{C}$  isotopologue, Fig. 1B.

Fig. 3A shows an experimental CW-EPR spectrum (solid black line) of a solution of  $^{13}\text{C}$ -**PTMTC** in DMSO ( $c = 1$  mM)

recorded at room temperature, and the corresponding simulation (dashed red line). The *g*-value,  $2.0028 \pm 0.0002$ , and effective isotropic hyperfine couplings were determined by simulation of the experimental spectra.<sup>32</sup>

The data for the  $^{13}\text{C}$  hyperfine couplings are presented in Table 1. The values are in accordance with data for natural abundance  $^{13}\text{C}$  couplings reported by Paniagua *et al.*<sup>30</sup> Sabacky *et al.*<sup>36</sup> reported hyperfine coupling values of two related radicals, *viz.* the unsubstituted triarylmethyl and 2,6,2',6',2'',6''-hexamethoxytriarylmethyl radicals. They had been enriched with  $^{13}\text{C}$  (56% and 54%, respectively) at the central carbon. The hyperfine coupling of the central carbon for the unsubstituted triarylmethyl radical was 64.46 MHz and 73.43 MHz for the 2,6,2',6',2'',6''-hexamethoxytriarylmethyl radical.<sup>36</sup>

### 3.3. Influence of pH on $^{13}\text{C}$ -**PTMTC** line width

Since the **PTMTC** radical bears an ionizable carboxyl group, it can be expected to show pH sensitivity. By varying pH, terminal groups are ionized from carboxylic acid at low pH to carboxylate at high pH and a mixture of both at pH values around the *pK*. Solutions of  $^{13}\text{C}$ -**PTMTC** ( $c = 1$  mM) in PB (50 mM, pH range from 2 to 12) were used to investigate the impact of pH on EPR spectral parameters such as line widths. The lowest and highest pH values were adjusted using pure HCl and NaOH solutions.

Remarkably, the observed hyperfine splitting and line widths were found to be independent of the solution pH. Only in very acidic solution (pH < 2) the EPR signal strength was reduced,

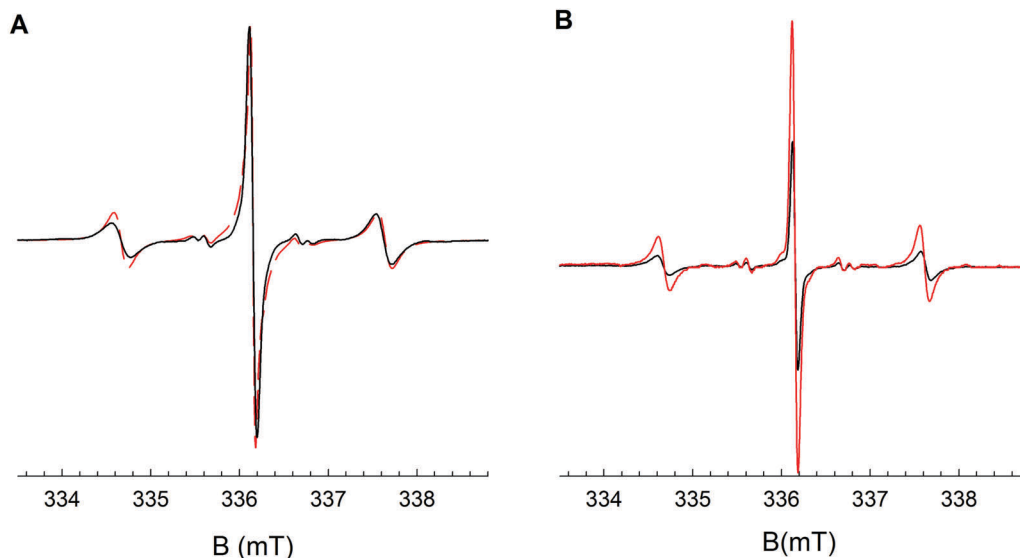


Fig. 3 (A) CW-EPR spectrum of  $^{13}\text{C}$ -PTMTC (1 mM in DMSO) recorded at room temperature. The experimental spectrum is shown in black (solid black line), the simulated spectrum in red (dashed red line). (B) CW EPR X-band spectra of  $^{13}\text{C}$ -PTMTC recorded at 37 °C for pH = 5.6 (red line) and pH = 1.0 (black line).

Table 1  $^{13}\text{C}$  hyperfine coupling values of  $^{13}\text{C}$ -PTMTC

$^{13}\text{C}$ hyperfine couplings (MHz)	
Central carbon	83.5
1-Phenyl $^{13}\text{C}$ bridgehead ( <i>ipso</i> )	34.9
2,6-Phenyl $^{13}\text{C}$ in <i>ortho</i> position	29.0
3,5-Phenyl $^{13}\text{C}$ in <i>meta</i> position	5.9

Hyperfine couplings are measured in absolute values. The estimated error of hyperfine coupling is  $\pm 0.1$  MHz.

simply because of precipitation, Fig. 3B. Importantly, at physiological pH values the samples were found to be stable for the duration of the experiments.

The negligible influence of pH can also be seen by following the ratio of the central  $^{12}\text{C}$  peak and of the  $^{13}\text{C}$  doublet line amplitudes at the low field (LF) and high field (HF) positions, respectively, Fig. 4. Between pH 2 and 12, the ratio is virtually constant, which is a clear indication that the unpaired electron spin distribution is not altered. A change in the ratio would be expected if changes in the electronic structure, potentially induced through protonation/deprotonation by varying pH, took place.

Hence *in vivo*, the effect of pH as such on line width and shape may be neglected, both for the central peak and the  $^{13}\text{C}$  hyperfine coupling lines. This is advantageous as it means that there is one parameter less to be considered, but disadvantageous since it corroborates that carboxylic acid moieties in trityl radicals are poor microsensors for pH.

The same negligible effect of pH on the EPR line width of tris(tetrathiaphenyl)methyl tricarboxylic acid radicals was observed in our previous study.<sup>31</sup>

#### 3.4. Influence of viscosity on $^{13}\text{C}$ -PTMTC line width

Different glycerol–water mixtures (0% to 80% glycerol in water, m/m) were used to prepare solutions of PTMTC and  $^{13}\text{C}$ -PTMTC

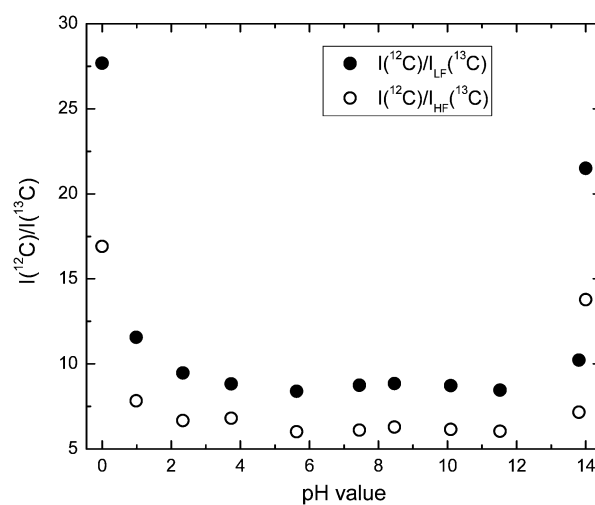


Fig. 4 Dependence of the ratio of peak-to-peak amplitudes of the central  $^{12}\text{C}$  line and  $^{13}\text{C}$  high field and low field doublet lines (filled circles,  $I(^{12}\text{C})/I_{\text{LF}}(^{13}\text{C})$ ; open circles,  $I(^{12}\text{C})/I_{\text{HF}}(^{13}\text{C})$ ) of  $^{13}\text{C}$ -PTMTC ( $c = 1$  mM) in PB (50 mM) on the pH value ranging from pH 2 to 12. Extreme pH values were adjusted using pure HCl and NaOH solutions.

( $c = 1$  mM). For PTMTC, between 10 and 40% (m/m) glycerol content, in aerated solutions a slight decrease in the EPR signal line width was detected (data not shown). This was most likely caused by the decrease in oxygen solubility with increasing percentage of glycerol,<sup>37</sup> whereas above 60% of glycerol (m/m), the increase in line width was dominated by the pronounced increase in viscosity. Apparently, viscosity by itself up to the value of about 40% of glycerol (m/m) has no effect on the EPR signal line width. This fact is important for *in vivo* applications as blood has a viscosity of 3–4 mPa s at 37 °C,<sup>38</sup> which is only reached at 44% of glycerol in water (m/m) at 20 °C.<sup>39</sup> As we found previously for this type of radical,<sup>31</sup> pH and viscosity can

be disregarded for *in vivo* EPR signals of this type of radical. However, microviscosity may play a role in matrices more complex than glycerol–water mixtures (including proteins, cell membranes, *etc.*). Reversible plasma protein binding, not studied here, will probably play a role, esp. for the very lipophilic esters of the radicals studied here. For tetrathiasubstituted trityl radicals, oxidative metabolism even led to covalent protein binding.<sup>40</sup>

Viscosity-dependent measurements (Fig. 5) were performed under aerated conditions, hence two contributions to linewidth are present: with increasing viscosity, rotational motion is slowed down, which is reflected in the low- and high-field lines of <sup>13</sup>C-PTMTC. Also, with higher viscosity collisional broadening by dissolved oxygen is reduced, which is visible in the reduction of line width with increasing viscosity in the central line. Apparently, the reduction of collisional broadening leads to a reduced linewidth and overcompensates for the small linewidth increase that was found for deoxygenated glycerol/water solutions.<sup>41,42</sup>

In contrast, viscosity did have significant influence on line width in the spectrum of the <sup>13</sup>C enriched radical. As depicted in Fig. 5, the doublet peak line widths were dominated by viscosity from the beginning. Indeed, beyond approx. 30% glycerol content, they became too broad for exact line width determination. So despite the fact that viscosity has no effect on PTMTC EPR signal line width up to a value of about 40% of glycerol, viscosity and viscosity changes of a medium can be observed through the ratio of the intensity of the central <sup>12</sup>C peak and the <sup>13</sup>C doublet line. A linear dependence was observed for line width ratio and temperature between 20 °C and 90 °C. The dependence for two temperatures only that are relevant for *in vivo* applications is shown in Fig. S1 (ESI<sup>†</sup>). The observable temperature effect (smaller peak ratio at higher temperature) is mainly due to viscosity changes and little contribution of oxygen loss with temperature.

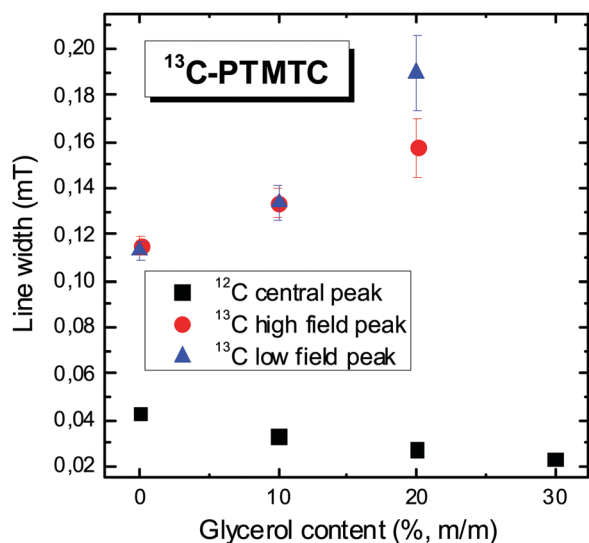


Fig. 5 Changes in peak to peak line width at different glycerol concentrations in aerated solution: <sup>13</sup>C-PTMTC (*c* = 1 mM). The <sup>12</sup>C peak (black squares) as well as the high field (red circles) and low field (blue triangles) peak of the <sup>13</sup>C doublet peak are shown.

### 3.5. Influence of oxygen on PTMTC line width

The EPR signal line width increase is directly proportional to the oxygen concentration.<sup>43</sup> A solution of PTMTC (*c* = 1 mM) in PB (50 mM, pH 7.4) shows a linear relationship between line width and oxygen concentration (Fig. 6). Again, we only considered the physiologically relevant range of oxygen content. It is important to note that the small slope of the curve is not primarily caused by an insensitivity of the radicals. It is simply due to the fact that in aqueous solution, the concentration of dissolved oxygen increases only very little with increasing oxygen partial pressure.<sup>44</sup>

The influence of oxygen was also studied in organic solvents. To examine the influence of solution parameters on the EPR signal, methanol was chosen as an example solvent. EPR spectra of methanol–water mixtures (10 to 100% methanol in water, V/V) including 1 mM of <sup>13</sup>C-PTMTC were investigated. In aerated solutions (Fig. 7A), with increasing MeOH concentration the line width of both the <sup>12</sup>C central peak and the doublet peak (<sup>13</sup>C radical signal) increased. This can be explained as follows: with increasing MeOH concentration, oxygen solubility increases,<sup>45</sup> leading to shorter relaxation times and, thus, broader lines because of the interaction between the paramagnetic oxygen and the spin probe. Under deoxygenated conditions (Fig. 7B), it was expected that the line width would not change because the oxygen effect was excluded. However, the line width of both <sup>13</sup>C-PTMTC doublet peaks increased up to approx. 50% MeOH and decreased beyond. This pattern follows the increase and decrease of viscosity of methanol–water mixtures.<sup>43</sup> The (slight) reduction, about 4%, of the line width of the <sup>12</sup>C-PTMTC signal follows the deviations reported for the water–methanol system such as volume contraction with its maximum at 56% of MeOH<sup>46</sup> as well as a parabolic entropy profile for both methanol and water in the methanol–water mixtures compared to the pure liquids.<sup>47</sup> It should also be noted that preferential solvation effects for radicals in methanol–water mixtures may be attributed to nonlinear behavior of the spectral parameters.<sup>48</sup> Similar trends can be observed by looking at the

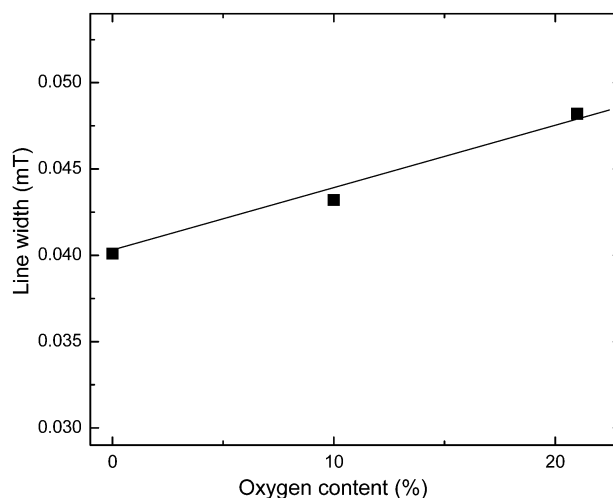


Fig. 6 Line width of the EPR signal of PTMTC (*c* = 1 mM) in PB (50 mM, pH 7.4) at different oxygen contents in the vapour phase. The straight line is only meant to guide the eye.

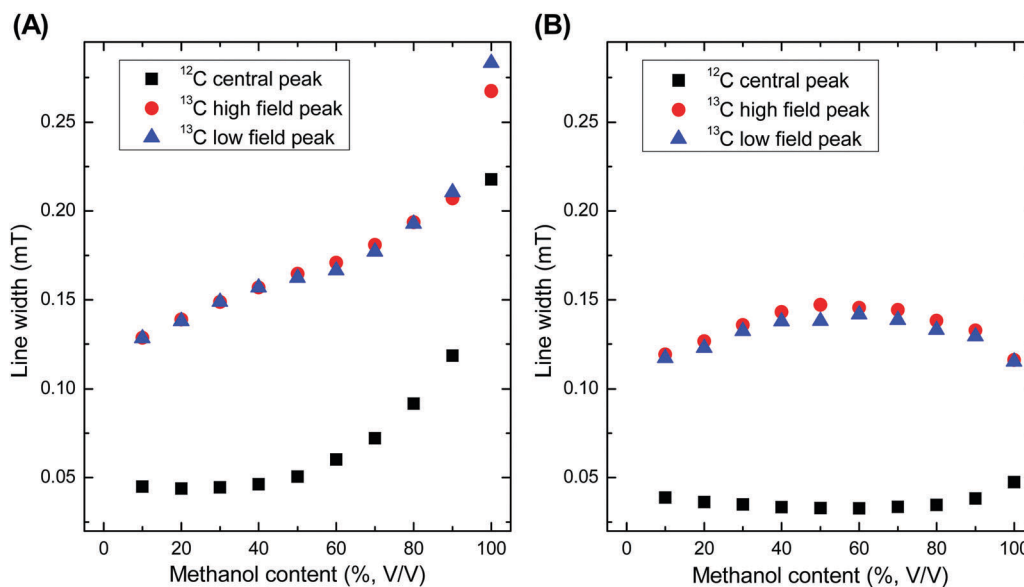


Fig. 7 Effect of increasing MeOH content on the line width of  $^{13}\text{C}$ -PTMTC ( $c = 1 \text{ mM}$ ); the central peak (black squares) as well as the high field (red circles) and low field (blue triangles) peak of the doublet peak are shown either under (A) aerobic conditions (20.9%  $\text{O}_2$ ) or (B) deoxygenated conditions ( $\approx 0\% \text{ O}_2$ ).

dependence of the  $1/T_M$  relaxation rate ( $1/T_M \sim \text{linewidth}$ ) on water-methanol compositions recorded at room temperature (see Fig. S2, ESI $^\dagger$ ). This effect is not evident for the  $1/T_M$  relaxation rates of  $^{13}\text{C}$ -PTMTC doublet peaks due to the stronger influence of other nuclear relaxation mechanisms including effects of viscosity.

### 3.6. Influence of temperature on $^{13}\text{C}$ -PTMTC line width

The effect of temperature on the intensity of the central PTMTC EPR peak is consistent with Curie's law, whereas the intensity of the  $^{13}\text{C}$  doublet shows more complex behaviour as can be seen in Fig. S3, ESI $^\dagger$ .

The effect of viscosity changes on the  $^{13}\text{C}$ -PTMTC signal is pronounced, leading concomitantly to an increase of the amplitude of both the HF and LF parts of the doublet by a factor of approx. 5 (data not shown) and a decrease of their line widths by a factor of approx. 3. The linear relation between the line width and the viscosity/temperature ratio as described by the Stokes-Einstein equation is depicted in Fig. 8. As can be expected, this linear behavior was not observed for the  $^{12}\text{C}$ -PTMTC line, where the lack of spectral anisotropy effectively leads to EPR spectra that show no dependence on rotational motion.

The linear viscosity/temperature relation indicates that for  $^{13}\text{C}$ -PTMTC, the rotational diffusion is the dominant effect on line width.<sup>49,50</sup> Importantly in view of potential applications, this allows for measurements of viscosity (in the local environment of the radical) even if other solvent parameters are also changed, e.g., oxygen content.

### 3.7. Radical stability

A solution of  $^{13}\text{C}$ -PTMTC ( $c = 1 \text{ mM}$ ) in PB (50 mM, pH 7.4) was used to test the long-term stability of the samples. Thermal annealing of solutions stored in the dark (to suppress decay pathways based on photochemical reactions) was performed to

study the changes in spectral parameters during accelerated aging.<sup>51</sup> In the temperature range of 323–353 K, the peak-to-peak amplitudes of the central line ( $I_{pp}$ ) were used to follow changes in the signal with time. As expected, the decrease in the EPR signal intensity was more pronounced at higher annealing temperatures. The EPR data presented in Fig. 9A were analyzed in terms of first-order kinetics:

$$\ln(I_{pp}/I_0) = -k(T) \cdot t, \quad (1)$$

where  $I_0$  is the peak height of the central line obtained at time  $t = 0$  from the first derivative of the spectrum, and  $k$  is the rate constant, which is a function of the absolute temperature,  $T$ . The kinetic parameters for the process ( $k_0$ ,  $\Delta E$ ) were derived by fitting the obtained rate constants  $k_i(T)$  to a simple Arrhenius-type equation

$$k(T) = k_0 \cdot e^{-\frac{\Delta E}{RT}}, \quad (2)$$

where  $k_0$  is the frequency factor,  $\Delta E$  is the activation energy, and  $R$  is the universal gas constant ( $R = 8.314 \text{ J mol}^{-1} \text{ K}^{-1}$ ). The Arrhenius plot of the derived rate constants (first order kinetics), from which the activation energies have been extracted, are shown in Fig. 9B. The resulting activation energy ( $\Delta E$ ) is  $226.5 \pm 16.9 \text{ kJ mol}^{-1}$ , and the frequency factor ( $\ln k_0$ ) is  $73.4 \pm 6.0 \text{ min}^{-1}$  ( $r^2 = 0.9889$ ). These data indeed indicate a long-term stability when radical solutions are stored properly, i.e. under dark conditions, as the radicals were not stable in solution after 24 h if kept in light (no data given).

Hence, for *in vivo* applications, long-term stability of the radicals can be assured when solutions are kept in the dark and at moderate temperatures, conditions that will normally be met. To test for stability against reducing agents, which of course can be seen as a crude measure of *in vivo* conditions, we investigated the reaction with ascorbic acid as a common

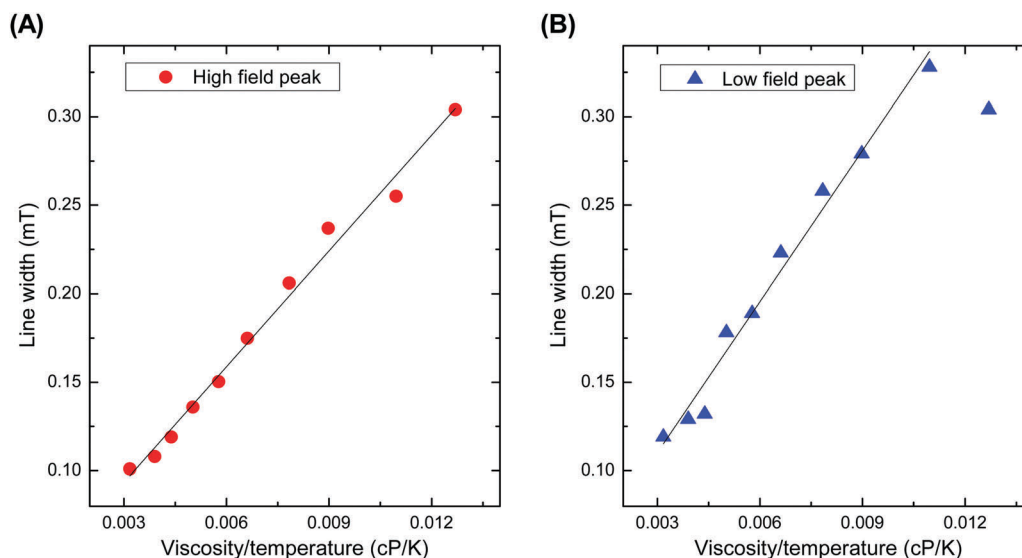


Fig. 8 Effect of temperature on line width. Solution of  $^{13}\text{C}$ -PTMTC ( $c = 1 \text{ mM}$ ) in glycerol/phosphate buffer 50 mM, pH 7.4 (40/60, V/V), measured from 20 to 70 °C: (A) HF peak (red circles); (B) LF peak (blue triangles). Straight lines are meant to guide the eye.

biological reducing agent. This is presented in the Fig. S4, ESI.† After approx. 60 min, half of the signal intensity had decayed. Despite this rather rapid decay, lifetimes on this order of magnitude may still be sufficient for *in vivo* imaging where other factors determine the time-span of EPR measurements, *e.g.*, for how long an animal can be maintained in a fixed position.

It was reported that the tetrathiaphenylmethyl radical Ox063 was stable in the presence of ascorbate, glutathione and NADPH. PTMTC was reported to be stable towards hydrogen peroxide (500  $\mu\text{M}$ ), alkyl peroxy radicals, hydroxyl radicals, nitric oxide, glutathione (1 mM), and ascorbate (100  $\mu\text{M}$ ). PTMTC reacts specifically with superoxide, causing decrease of EPR signal

intensity. The reaction with superoxide involved a reduction of PTMTC radical into  $\alpha\text{H}$ -PTMTC unlike the reaction with tetrathia-TAM radicals which was an oxidation process into the cation.<sup>19</sup> In general, tetrachlorotrimethyl radicals are more stable towards oxidation, while tetrathiatriethyl radicals are more stable towards reduction.

### 3.8. Radical stability in cell extracts

With the help of cell lysate experiments, *in vivo* conditions can be mimicked even better and radical degradation can be quantified. We used a *Xenopus laevis* oocyte cell extract. The *Xenopus laevis* oocytes trial is an established and easy-to-use model system to perform microinjection experiments. In our

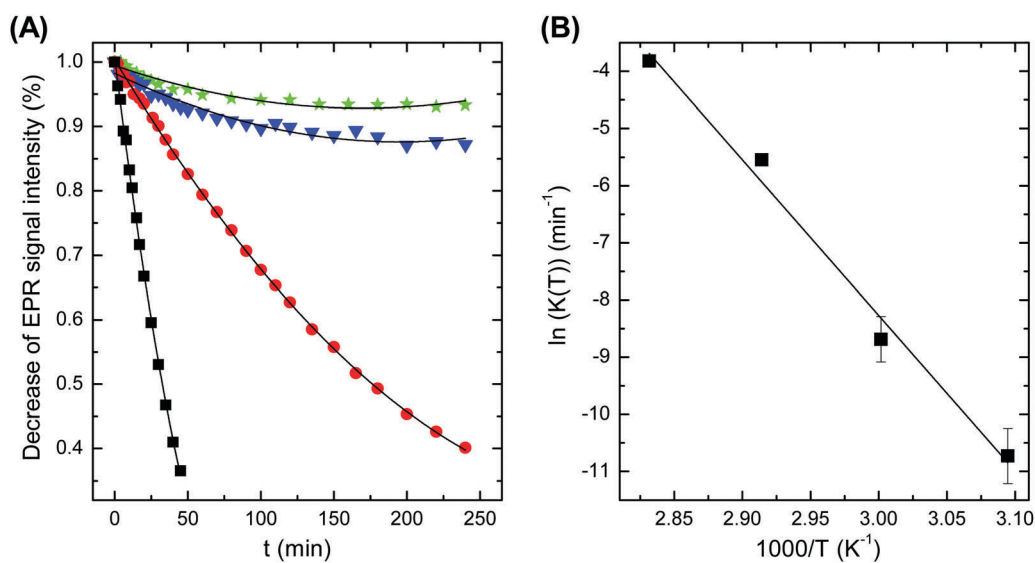


Fig. 9 (A) Thermal decay of  $^{13}\text{C}$ -PTMTC sample stored at different elevated temperatures: 353.15 K,  $r^2 = 0.9922$  (black squares); 343.15 K,  $r^2 = 0.9847$  (red circles); 333.15 K,  $r^2 = 0.9999$  (blue triangles); 323.15 K,  $r^2 = 0.9987$  (green stars). The solid lines represent monoexponential fits to eqn (1). (B) Rate of radical decay as a function of temperature.

experiment, 5  $\mu\text{l}$  of the 0.5 mM solution of **PTMTC** in PB (50 mM, pH 7.4) was mixed with 15  $\mu\text{l}$  of the cell lysate and was vortexed for 10 seconds and measured in a capillary ring cap. The EPR signal of **PTMTC** has a half-life of less than ten minutes. This indicates that encapsulation or some other means of protection will be advantageous *in vivo*, e.g., in polymeric or small molecule carriers. The encapsulation was described and investigated in more detail in ref. 31. With **PTMTC** it had been shown that in human blood or plasma, a 40% decrease of the signal intensity occurred after 30 min only.<sup>19</sup> So while tetrachloro-TAM radicals are more resistant to oxidation (shelf-life of several years if kept from light), they are more easily reduced in comparison to tetrathia-substituted TAMs.

## 4 Conclusion

Among stable trityl radicals with a single line in the EPR spectrum, perchlorinated trityl radicals are relatively easy to prepare from readily available starting materials in just three steps, including the possibility of <sup>13</sup>C labelling of the central carbon atom. **PTMTC** is distinguished by a single rather narrow EPR line, attractive for *in vivo* applications including imaging, where a strong signal is mandatory. However, the lack of anisotropy of the spectrum (in particular hyperfine interactions) limits spectroscopic conclusions or makes line width and shape changes ambiguous as to what causes them. We show that pH and macroviscosity can be disregarded *in vivo*, while there is a clear but—due to small oxygen solubility changes with increasing partial pressure—weak oxygen dependence of the line width in aqueous solutions. As long as the radical is not exposed to light, it is stable even in solution. However, since it quickly reacts with reducing agents (ascorbic acid or in cell lysate), this type of radical can only be used in a formulation that will protect it. Partial isotope labelling of **PTMTC** leads to its isotopologue <sup>13</sup>C-**PTMTC**, a radical with practically identical physicochemical parameters but a different EPR spectrum. In particular, effects of changes in rotational motion (viscosity) are observable in <sup>13</sup>C-**PTMTC** and can be analyzed. Since the partial (50%) isotope-labelling allows for a simultaneous detection of <sup>12</sup>C-**PTMTC** and the pure <sup>13</sup>C-**PTMTC** EPR signals, it combines benefits of *in vivo* and imaging applications (<sup>12</sup>C-**PTMTC**) with the possibility to obtain deeper insights into the local, nanoscopic environment (<sup>13</sup>C-**PTMTC**). Hence, this mixture of isotopic radicals could gain importance as a probe for both types of parameters (viscosity and oxygen concentration) and applications in, e.g., spectral-spatial imaging. The problem of toxicity will not be an issue when and if the radicals are incorporated in lipophilic nano- or microcapsules<sup>31</sup> with slower release than metabolic reduction after release.

## Acknowledgements

We would like to thank Dr Dieter Ströhl (MLU Halle) for NMR analyses, Dr Christian Ihling (MLU Halle) for HRMS measurements, and Ms Heike Rudolf (MLU Halle) for IR measurements.

This research was supported by Deutsche Forschungsgemeinschaft (DFG) (MA 1648/8 to K. M. and DR 1024/1-1 to S. D.), the Egyptian Ministry of Higher Education and Scientific Research and the Institut fuer Angewandte Dermatopharmazie (IADP) Halle.

## References

- 1 Y. Liu, F. A. Villamena and J. L. Zweier, *Chem. Commun.*, 2008, 4336.
- 2 B. Driesschaert, V. Marchand, P. Levêque, B. Gallez and J. Marchand-Brynaert, *Chem. Commun.*, 2012, **48**, 4049.
- 3 K. Mäder, B. Bittner, Y. Li, W. Wohlauf and T. Kissel, *Pharm. Res.*, 1998, **15**, 787.
- 4 R. Ahmad and P. Kuppusamy, *Multifrequency Electron Paramagnetic Resonance*, Wiley-VCH Verlag GmbH & Co. KGaA, 2011, p. 755.
- 5 B. B. Williams and H. J. Halpern, *Biomedical EPR, Part A: Free Radicals, Metals, Medicine, and Physiology*, Springer, 2005, p. 283.
- 6 M. Gomberg, *J. Am. Chem. Soc.*, 1900, **22**, 757.
- 7 P. Jacobson, *Ber. Dtsch. Chem. Ges.*, 1905, **38**, 196.
- 8 H. Lankamp, W. T. Nauta and C. MacLean, *Tetrahedron Lett.*, 1968, **9**, 249.
- 9 J. Schmidlin, *Ber. Dtsch. Chem. Ges.*, 1908, **41**, 2471.
- 10 E. G. Janzen, F. J. Johnston and C. L. Ayers, *J. Am. Chem. Soc.*, 1967, **89**, 1176.
- 11 M. Gomberg, *J. Am. Chem. Soc.*, 1901, **23**, 496.
- 12 M. Ballester, *Pure Appl. Chem.*, 1967, **15**, 123.
- 13 M. Ballester, J. Riera-Figueras, J. Castaner, C. Badfa and J. M. Monso, *J. Am. Chem. Soc.*, 1971, **93**, 2215.
- 14 M. Ballester, J. Castaner, J. Riera, A. Ibanez and J. Pujadas, *J. Org. Chem.*, 1982, **47**, 259.
- 15 M. Ballester, J. Riera, J. Castaner, A. Rodriguez, C. Rovira and J. Veciana, *J. Org. Chem.*, 1982, **47**, 4498.
- 16 A. Bratasz, A. C. Kulkarni and P. Kuppusamy, *Biophys. J.*, 2007, **92**, 2918.
- 17 G. Meenakshisundaram, E. Eteshola, A. Blank, S. C. Lee and P. Kuppusamy, *Biosens. Bioelectron.*, 2010, **25**, 2283.
- 18 V. Dang, J. Wang, S. Feng, C. Buron, F. A. Villamena, P. G. Wang and P. Kuppusamy, *Bioorg. Med. Chem. Lett.*, 2007, **17**, 4062.
- 19 V. K. Kutala, F. A. Villamena, G. Ilangovan, D. Maspoeh, N. Roques, J. Veciana, C. Rovira and P. Kuppusamy, *J. Phys. Chem. B*, 2008, **112**, 158.
- 20 J. Wang, V. Dang, W. Zhao, D. Lu, B. K. Rivera, F. A. Villamena, P. G. Wang and P. Kuppusamy, *Bioorg. Med. Chem.*, 2010, **18**, 922.
- 21 J. A. Mesa, S. Chávez, L. Fajará, J. L. Torres and L. Juliá, *RSC Adv.*, 2013, **3**, 9949.
- 22 M. Ballester, J. Riera, J. Castaner, C. Rovira, J. Veciana and C. Onrubia, *J. Org. Chem.*, 1983, **48**, 3716.
- 23 F. M. Vigier, D. Shimon, V. Mugnaini, J. Veciana, A. Feintuch, M. Pons, S. Vega and D. Goldfarb, *Phys. Chem. Chem. Phys.*, 2014, **16**, 19218.
- 24 D. Banerjee, J. C. Paniagua, V. Mugnaini, J. Veciana, A. Feintuch, M. Pons and D. Goldfarb, *Phys. Chem. Chem. Phys.*, 2011, **13**, 18626.

- 25 C. Gabellieri, V. Mugnaini, J. C. Paniagua, N. Roques, M. Oliveros, M. Feliz, J. Veciana and M. Pons, *Angew. Chem., Int. Ed.*, 2010, **49**, 3360.
- 26 M. Oliveros, L. González-García, V. Mugnaini, F. Yubero, N. Roques, J. Veciana, A. R. González-Elipe and C. Rovira, *Langmuir*, 2011, **27**, 5098.
- 27 D. Maspoch, D. Ruiz-Molina, K. Wurst, C. Rovira and J. Veciana, *Chem. Commun.*, 2004, 1164.
- 28 D. Maspoch, N. Domingo, D. Ruiz-Molina, K. Wurst, J. Tejada, C. Rovira and J. Veciana, *C. R. Chim.*, 2005, **8**, 1213.
- 29 V. Mugnaini, M. Paradinas, O. Shekhah, N. Roques, C. Ocal, C. Woll and J. Veciana, *J. Mater. Chem. C*, 2013, **1**, 793.
- 30 J. C. Paniagua, V. Mugnaini, C. Gabellieri, M. Feliz, N. Roques, J. Veciana and M. Pons, *Phys. Chem. Chem. Phys.*, 2010, **12**, 5824.
- 31 J. Frank, M. Elewa, M. M. Said, H. A. El Shihawy, M. El-Sadek, D. Müller, A. Meister, G. Hause, S. Drescher, H. Metz, P. Imming and K. Mäder, *J. Org. Chem.*, 2015, **80**, 6754.
- 32 S. Stoll and A. Schweiger, *J. Magn. Reson.*, 2006, **178**, 42.
- 33 D. Maspoch, N. Domingo, D. Ruiz-Molina, K. Wurst, G. Vaughan, J. Tejada, C. Rovira and J. Veciana, *Angew. Chem.*, 2004, **116**, 1864.
- 34 M. Ballester, J. Riera, J. Castañer, C. Rovira and O. Armet, *Synthesis*, 1986, 64.
- 35 N. Roques, D. Maspoch, K. Wurst, D. Ruiz-Molina, C. Rovira and J. Veciana, *Chem. – Eur. J.*, 2006, **12**, 9238.
- 36 M. Sabacky, C. Johnson, R. Smith, H. Gutowsky and J. Martin, *J. Am. Chem. Soc.*, 1967, **89**, 2054.
- 37 B. B. Williams, H. al Hallaq, G. Chandramouli, E. D. Barth, J. N. Rivers, M. Lewis, V. E. Galtsev, G. S. Karczmar and H. J. Halpern, *Magn. Reson. Med.*, 2002, **47**, 634.
- 38 G. Elert, *The Physics Hypertextbook*, 2005.
- 39 *CRC handbook of chemistry and physics*, (Internet Version 2009), CRC Press/Taylor and Francis, Boca Raton, FL, 89th edn, 2009.
- 40 C. Decroos, J.-L. Boucher, D. Mansuy and Y. Xu-Li, *Chem. Res. Toxicol.*, 2014, **27**, 627.
- 41 L. Yong, J. Harbridge, R. W. Quine, G. A. Rinard, S. S. Eaton, G. R. Eaton, C. Mailer, E. Barth and H. J. Halpern, *J. Magn. Reson.*, 2001, **152**, 156.
- 42 R. Owenius, G. R. Eaton and S. S. Eaton, *J. Magn. Reson.*, 2005, **172**, 168.
- 43 W. M. Haynes, *CRC handbook of chemistry and physics*, CRC press, 2012.
- 44 R. Ahmad and P. Kuppusamy, *Chem. Rev.*, 2010, **110**, 3212.
- 45 I. Kutsche, G. Gildehaus, D. Schuller and A. Schumpe, *J. Chem. Eng. Data*, 1984, **29**, 286.
- 46 L. Dougan, S. Bates, R. Hargreaves, J. Fox, J. Crain, J. Finney, V. Reat and A. Soper, *J. Chem. Phys.*, 2004, **121**, 6456.
- 47 T. A. Pascal and W. A. Goddard III, *J. Phys. Chem. B*, 2012, **116**, 13905.
- 48 J. Heller, H. Elgabarty, B. Zhuang, D. Sebastiani and D. Hinderberger, *J. Phys. Chem. B*, 2010, **114**, 7429.
- 49 L. Burlamacchi, *Mol. Phys.*, 1969, **16**, 369.
- 50 P. Atkins and D. Kivelson, *J. Chem. Phys.*, 1966, **44**, 169.
- 51 K. C. Waterman and R. C. Adami, *Int. J. Pharm.*, 2005, **293**, 101.